Self-assembled concentric stripes of diamond particles by a pinning-depinning mechanism

Paulina Czarnecka-Trela [a,*], Adam M. Wojciechowski [a], Mariusz Mrózek [a], Maciej J. Głowacki [b], Robert Bogdanowicz [b], Wojciech Gawlik [a,*]

[a] Institute of Physics, Jagiellonian University, Łojasiewicza 11, 30-348 Krakow, Poland
[b] Department of Metrology and Optoelectronics, Faculty of Electronics, Telecommunications and Informatics, Gdansk University of Technology, Narutowicza 11/12, 80-233 Gdansk, Poland

ARTICLE INFO

ABSTRACT

We describe the novel mechanism of spontaneous formation of the concentric stripe patterns of microdiamonds via gradual solvent evaporation from a suspension confined in a teardrop well. The self-organized patterns exhibit a series of arcs with regular spacings varying between hundreds of micrometers and millimeters. They result from an interplay between the directional forced circulation of the solvent and a stick-slip movement of its contact line during the gradual drying of the suspension. We reveal the mechanism of the phenomenon and discuss the effects of various parameters on the obtained structures.

1. Introduction

Numerous studies over the last decades have focused on the interplay between evaporation and particle deposition. Evaporation as a method to control small particle assemblies (from molecules to colloids) appears to be a promising and rather simple technique for the fabrication of regular patterns of deposited particles [1–6].

Evaporation-related patterns are useful as an efficient and economical method for self-assembly techniques [7] and the construction of device-oriented structures [8,9]. They are also important for the reduction of print and coating inhomogeneities [8,10,11] and for the production and control of specific structures that allow controlled surface functionalization [12]. The latter also includes the self-assembly during the evaporation of liquid suspensions. In these processes, the capillary bridge [13,14] creates a meniscus at the contact line, and a stick-slip motion of its interface produces regular quasi-periodic stripe patterns [7] like the concentric ring patterns reported in many studies [1,14–16].

Well-known examples of such patterns are *coffee rings* which arise due to capillary and Marangoni flows in freely evaporating suspensions of insoluble particles [17–20]. They have a powerful impact on the spatial distributions and properties of the nanoparticle deposits obtained [7,14,16,21–25].

The colloidal behavior of diamond particles (DPs) depends not only on the properties of the particles but also on the chemical composition and pH of the dispersion medium [26]. The discovery of spontaneous self-assembly of the DPs has shed new light on the colloidal properties of these particles. One of the factors inducing or preventing the self-assembly of DPs is their surface moieties. Jirásek et al. [27] found that hydrogenated detonation nanodiamonds (DNDs) functionalized with reactive oxygen species tend to self-assemble into chain-like structures after deposition on Si substrates, contrary to non-functionalized hydrogenated DNDs. Chang et al. [28] reported that DNDs suspended in water without any surfactants tend to dynamically form lace-like networks rather than remain single particles. Yoshikawa et al. [29] proved that this self-assembly could be prevented by coating the particles with polyglycerol and increasing the ionic strength of the dispersion medium. El-Demrdash et al. [30] showed that the sizes and shapes of agglomerates spontaneously self-assembled from DNDs in water are significantly affected by the concentration of the diamond particles, while the salt content (NaCl) in the range of 0.005–1 mM has a negligible influence. Opletal et al. [31] applied molecular dynamics simulations to verify the impact of the morphologies, polydispersity, and surface potentials of the DPs on the outcomes of the self-assembly of the particles in a vacuum.

In many cases, self-assembly of the DPs is specifically engineered and deliberately induced to develop controllable arrangements of the particles or to create novel hybrid particles. Shulevitz et al. [32] trapped 40 nm-sized, nitrogen vacancy (NV) centers-containing DPs from an aqueous suspension in cylindrical traps manufactured in a polymer template via electron beam lithography. The removal of the template has left an array of evenly distributed diamond particles, enabling automated characterization of the optical properties of the NV centers. Li et al. [33] used self-assembling to integrate combretastatin A4 with DPs functionalized by protamine sulfate. The resulting biocompatible complexes enabled the combination of anti-angiogenesis therapy with photothermal therapy against liver cancer. Hybridization of complementary sequences of DNA was used by both Liang et al. [34] and Schmidheini et al. [35] to create conjugates of gold nanoparticles and fluorescent DPs via self-assembling with the aim of enhancing the emission dynamics of NV centers through the localized surface plasmon resonance of gold.

The present paper deals with the mechanism for the formation of diamond micro- and nanocrystal patterns generated through the evaporation of liquid confined within a "teardrop" microslide cavity. The coverslip eliminated the evaporation above the cavity wall, thus the process occurred only at its edge from a thin layer of liquid between glass surfaces. After evaporation of the solvent, specific patterns were present at the bottom of the cavity. We analyze their characteristics for different solvents. The observed patterns depend on various parameters, such as the size of the diamond, solvent, and cavity geometry. This paper describes the novel mechanism that leads to the formation of the stripe patterns and discusses the dependence of their properties (number of stripes, length, and spacings) on various factors. It resembles the arrangement utilizing a capillary bridge described in [13] yet with several important differences: in our setup, we have an opposite geometry to that of [13,14], the evaporation rate is not regular, and most importantly, the dynamics of the process is controlled by a directional geometry-determined suspension circulation, which dominates other flows in the liquid.

Our study elucidates a direct correlation between the unique surface chemistry and the behavior of diamonds and its impact on material properties. The microcrystalline diamond particles analyzed here display stochastic morphologies, a direct result of the ball milling process. This contrasts with other nanoparticles, often characterized by uniform shapes conducive to isotropic self-assembly processes, both chemical and physical, which are less prevalent in diamond structures. Central to our investigation is the observation of the dynamic surface modifications in diamond particles. These modifications are attributed to oxidation and deprotonation processes, markedly altering the stability and zeta potential. Such alterations significantly impact the assembly behavior of these particles, a phenomenon intrinsically associated with distinct diamond's characteristics [36–39].

2. Materials and methods

We used sub-micrometer DPs suspensions made in-house from particles obtained by disintegration of fluorescent diamond powder (MDNVN1umHi, Adamas Nanotechnologies Inc.) with a dominant particle size fraction equal to 700–750 nm. The ultrasonic disintegration of diamonds in the solvents was carried out using a Bandelin Sonopuls HD 4200 homogenizer (Berlin, Germany). No abrasive has been used in the process, allowing particles to be crushed only as a result of collisions between them. The suspensions were prepared by 20 min long high-power pulsed ultrasound sonication (50 % duty cycle), which disintegrated the DPs aggregates while having a marginal effect on the mean grain size.

The suspensions were prepared using four different solvents: methanol (purity: ≥99.9 % A.C.S grade), isopropanol (purity: ≥99.9 % A.C·S grade), ethanol (purity: 96 %, ethanol-water solution) and deionized water. Each suspension that we used had an DPs mass concentration of

0.1 %. Although we mainly worked with sub-micrometer DPs, we also used the 140-nm size suspension (NDNV140nmMd-1.5 ppm-10 ml, Adamas Nanotechnologies Inc., Raleigh, NC, USA) to verify the effect of the diamond size on the results of the experiment.

Particle size distribution (PSD) in each suspension used in this study was measured via dynamic light scattering (DLS) with the Zetasizer Nano ZS particle analyzer (Malvern Panalytical, UK) equipped with a 633 nm laser. The analyzer is suitable to measure size distributions for particles with diameters in the range of 0.3 nm–10 μm [40]. Each suspension was measured in the backscatter configuration (light collected at an angle of 173°) and measurements were repeated 3 times. The Zetasizer Nano ZS has also been used to evaluate zeta potentials of the diamond particles dispersed in different liquids. For that purpose the suspensions were placed in standard, disposable folded capillary cells (DTS1070).

A microscope glass slide (25 × 76 mm in size and 1 mm in thickness) with a spherical cap cavity with a diameter of 15 mm and a depth equal to 0.41 ± 0.01 mm was filled with 40 μl of suspension. To confine the liquid, the standard 22 × 22 mm coverslip of 0.13–0.17 mm thickness was pulled over the well, taking care to avoid trapping air bubbles. Since the cover glass did not perfectly seal the cavity, the evaporation was confined but not eliminated and proceeded with a low rate determined by the imperfections of the glass surface contact (Suppl. Mater. Video 1 – Preparation).

The deposited patterns were observed with optical microscopy with white-light illumination (DNT DigiMicro Profi USB 5 Mpx) and scanning electron microscopy (SEM) (HITACHI S-4700 microscope with the NORAN Vantage microanalysis system). Due to relatively low deposit density, the light intensity scattered off the diamond particles can be taken as the measure of the scatterer's density, that is, in the first approximation, they represent the particle density. The dewetting and pattern formation processes were also recorded by the microscope camera (Moticam 2) and the recorded images and movies were analyzed with image analysis software (ImageJ). Experiments were carried out in air at room temperature (around 22 °C).

3. Results

The most important stages of the sample evolution on a time scale of minutes to hours are described below.

3.1. Mechanisms of the pattern formation

The main steps of pattern formation are schematically illustrated in Fig. 1. The liquid trapped in sealed well evaporates slowly at the edge of the cavity. Since the glass surfaces of a coverslip and a microslide are not perfectly flat and well-matching, the capillary force at the edge of the well has different values depending on the size of these imperfections. Small air bubbles enter the well at the spot where the capillary forces are the weakest, breaking the rotational symmetry around the edge of the cavity. The position of the bubble stream entrance spot is specific for each sample and generally remains stable over the entire evaporation cycle (except for <5 % of cases). The air-bubble stream moves DPs from the bottom of the well creating the inlet channel – a straight line region without DPs. Circulation forced by the directional air-bubble stream along the inlet channel moves DPs towards the tip of the contact angle shown by the arrow in Fig. 1b, where they accumulate and pin the contact liquid-air line. Simultaneously, the solvent evaporates and the central bubble keeps expanding. Since its contact line is pinned, the DPs are further deposited at the tip of the meniscus wetting angle and form a ring/arc-shape "rib" (Suppl. Mater. Video 2 – Inlet channel). Generally, the first rib constitutes a nearly full ring, since it is caused by a complete circumfluence of the big central bubble by the small-bubble flow. Eventually, the forces on the contact line overcome the pinning force, and the contact line jumps abruptly to the next equilibrium position placed closer to the perimeter of the well (Fig. 1c).

After the formation of the first rib, the phenomenon exhibits regular repetitive dynamics with the key role played by the pinning-depinning, or the stick-and-slip mechanism, similar to that observed in other studies, e.g. [1,4,22,25,41] This dynamics is determined by the competition between the forces on the contact line of the liquid ring around the central bubble and the pinning force, or by the properties of the so-called capillary bridge [13]. Each repetition of this mechanism creates another rib in the observed pattern (Fig. 1c).

Fig. 2(a) depicts a photograph of a typical pattern that appears during the evaporation of DPs suspension in isopropanol (IPA) and exhibits features related to all the stages discussed above. More details are visible in the attached movies. Fig. 2(b) and (c) shows the SEM image and the fluorescence scan image, respectively, of an expanded section of the stripe pattern depicted in Fig. 2(a).

3.2. Pinning-depinning (stick & slip) mechanism

The observations described above are manifestations of a special type of capillary effect, the capillary bridge that is described by the Laplace equation [42–44]. For the capillary bridge, it can be assumed that the stick-slip motion emerges from a competition between the force generated by the Laplace pressure and the anchoring friction force caused by the defects of the solid surface [45], in particular, the DPs deposit as in our case. The contact line pinning depends on the local concentration of the suspension the evaporation conditions and the particular influx rate of small air bubbles [46]. While the above references describe the salient features of the effect [42–45], in this work we focus on the qualitative description of the effect, with a particular emphasis on general pattern symmetry and morphology described in Section 3.3 and critical parameters such as particle size and solvent colloidal stability (Sections 3.3.2 and 3.3.3).
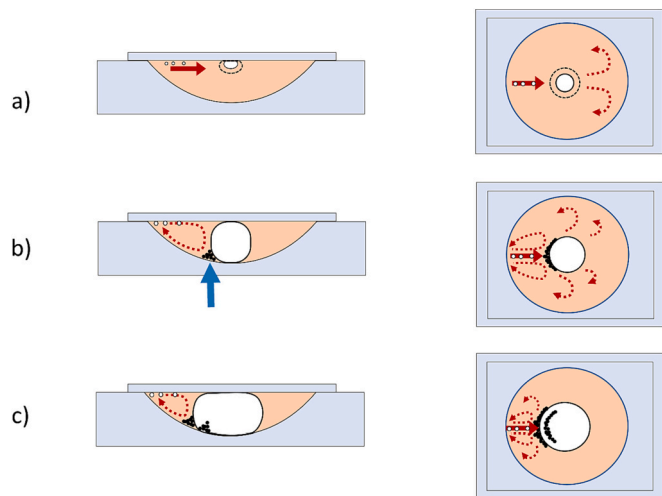

Fig. 1. Schematic of various stages of the solvent evaporation and formation of the DPs patterns. The left column shows cross-sections through the cavity and the cover slip; right – the top view. The orange color marks the liquid. Red arrows indicate liquid circulation within the cavity forced by air bubble stream, white dots symbolize air bubbles, and black dots the DPs deposit.
(a) small air bubbles (white dots) stream along the inlet channel towards the center of the cavity as shown by the red arrow and the central air bubble increases.
(b) after the central air bubble touches the bottom of the cavity, the air-liquid meniscus is formed. Air bubbles streaming towards the center create directional flow in the liquid that deposits DPs (black dots) at the tip of the wetting angle of the meniscus (shown by blue solid arrow).
(c) the stick and slip movement: the deposited DPs pin the liquid to the cavity bottom, yet the volume of the air bubble and strength of the capillary force keep increasing until the contact line of the expanding central bubble jumps to a new position where it is pinned again.
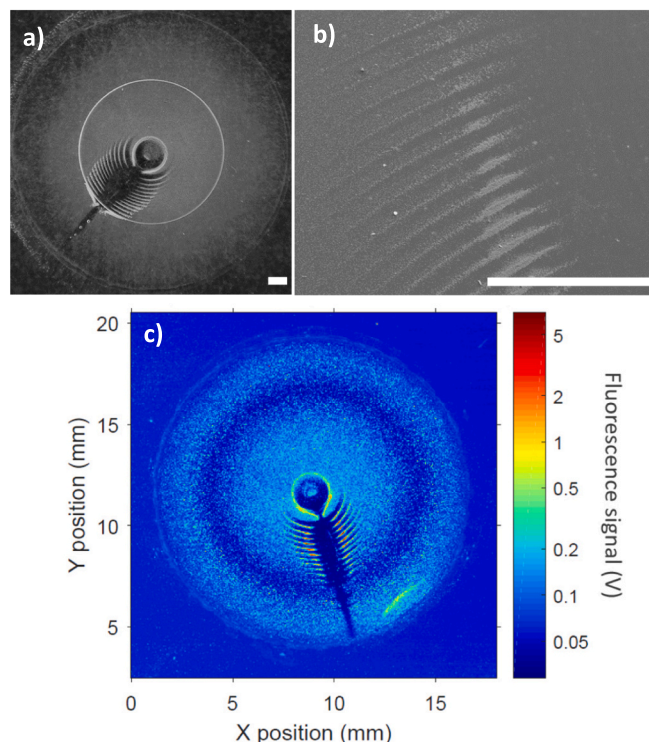

Fig. 2. Typical example of incomplete evaporation of DPs suspension in IPA: a) photograph illustrating the main stages of the evaporation patterns. Well-visible are: an inlet channel with individual small bubbles, the central air bubble, the developed rib structure, and a significant broadening of the inlet channel around the skeleton; b) SEM image with typical example of concentric stripe-patterns of diamonds; c) fluorescence scan image recorder on a confocal optical microscope setup. The size of the scale bar (white line) is 1 mm.

The evaporation of the solvent and the influx of small air bubbles into the cavity result in the expansion of the central bubble. Such an expansion moves the DPs deposit on the bottom of the well, the so-called, plough effect. It is associated with an increase in friction force on the contact line between three phases: air, DPs suspension, and glass well surface. The contact line moves slowly, slips, and the wetting angle at the contact line increases. Eventually, all forces are balanced and the contact line becomes stick or pinned by the diamond deposit at the bottom of the well. After pinning, the air-bubble pressure keeps increasing, and at some point the pinned contact line exerts a fast slip movement to a new equilibrium position, where it may be pinned again. Thus, the observed phenomenon results from a competition of all relevant forces: the capillary force, air pressure, and friction which lead to a repeated sequence of slip and stick movement that create the observed self-organized patterns of DPs deposit.

Thus, two kinds of slips may occur, the slow one, when the contact line is not pinned, or the rapid one, otherwise (Fig. 3). They both have been observed in our experiments: the slow slip is conveniently visible when the influx rate is low (Suppl. Mater. Video 3 – Slow slip) and one observes a systematic slow increase of the central bubble size without substantial change of the DPs distribution in the cavity, that is almost no rib movement. On the other hand, the quick slip (Suppl. Mater. Video 4 – Quick slip) occurs when a larger portion of air bubbles is injected into the central bubble. It is associated with an abrupt jump-like increase of the central bubble, vigorous rearranging of the DPs distribution, and formation of a new rib (Suppl. Mater. Video 4 – Quick slip).

3.3. Morphology of the deposited patterns

3.3.1. General pattern symmetry
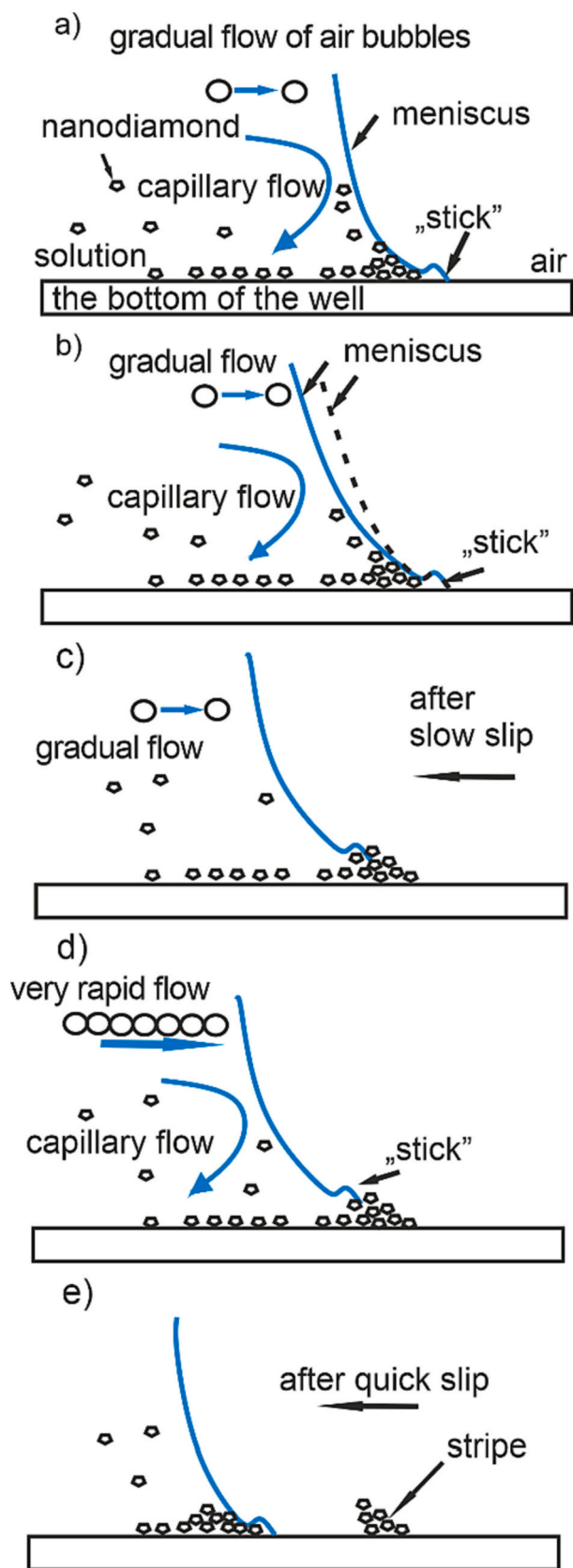The mechanisms discussed above are responsible for the specific fish

Fig. 3. Stick-slip movement of the contact line. Scenario for the stripe pattern formation similar to that described by Chen et al. [46]

skeleton-like appearance of the DPs patterns obtained after complete evaporation. The deposited pattern depends on many parameters, some well controlled, like the organized geometry, size of the DPs, and the kind of the solvent, but others are rather erratic in the experiment performed where the uncontrolled evaporation rate seems to be the most relevant factor. Despite the irregularity of the evaporation rate, >70 % of about 70 investigated samples characteristic structures with specific symmetry are well visible and characterized by three elements:

   i) a straight, empty line determined by the directional flow of air bubbles and the forced circulation of the suspension particles in the inlet channel that constitutes the skeleton's "spine";

   ii) arched stripes, which form the ribs of the skeleton. They are the result of the deposition of DPs and the stick-slip mechanisms discussed above (see Fig. 2(b));

   iii) a "head" formed by the circumfluence of the first central air bubble, according to Fig. 1(b).

3.3.2. Typical evaporation patterns and solvent effect

Once established, the directional flow remained stable for the entire evaporation cycle except for a few cases (<5 %) when a change in the entrance position of the inlet channel was observed (Fig. 4). The inlet channel (the skeleton's spine) was broadened by the backward circulation (recoil) from the central bubble (Suppl. Mater. Video 5 – Circulation) with a broadening degree strongly dependent on the kind of solvents: isopropanol, methanol, ethanol, and water. As seen in Fig. 5, the observed patterns demonstrated a strong dependence of their morphology on the type of solvent.

Qualitatively, the structures observed with isopropanol (IPA) (Fig. 5 (a)) had regular shapes of repetitive symmetrical arched skeleton ribs and were most stable and reproducible. They illustrated the mechanisms discussed above (Sections 3.1, 3.2) with the highest accuracy.

The patterns obtained with methanol (Fig. 5(b)) also exhibited a distinct fish skeleton-like structure with the spine and ribs, but the ribs were wider and less regular than those of IPA, and had irregular broken ends and visible gaps. Most likely, this resulted from a more dynamic recoil effect of the central bubble after a quick slip. Its consequence was a significant broadening of the input channel and a barely visible rib structure around the center of the well. The ends of the ribs are broadened by pushing the deposit through the slipping interface (a "plough effect" - Suppl. Mater. Video 5 – Circulation). The ribs that were more distant from the center were less distorted by the recoil effects and better visible.

The most characteristic feature of the ethanol patterns (Fig. 5(c)) were the ribs in the form of regular concentric rings broken by a well-visible, regular spine without DPs. The almost perfect circular stripes demonstrated that, in ethanol, the DPs completely circumfluent the central bubble. Moreover, there is a visible modulation of the amplitude of the stripes, which may be caused by some liquid oscillations before complete evaporation.

The patterns seen with the water suspensions (Fig. 5(d,e)) differed most strongly from the other ones. In particular, they did not show regular and symmetric patterns similar to those of fish skeleton-like structures. Instead, they had rather a chaotic shape. The patterns recorded with sub-micron DPs suspension exhibited some repeatability, but those seen with 140 nm DPs showed just a single ring with short fingers or spokes, similar to that described in Weon and Je [47]

Fig. 6 presents two typical rib profiles measured with IPA. The depicted profiles represent the distribution of the scattered light intensity with white-light illumination. They were measured along the broken lines marked in the insets to indicate the highest fringe (rib) contrast. As seen in both plots, the fringe contrast reaches nearly 100 %, which demonstrates very efficient modulation of the DPs density by the revealed mechanisms.
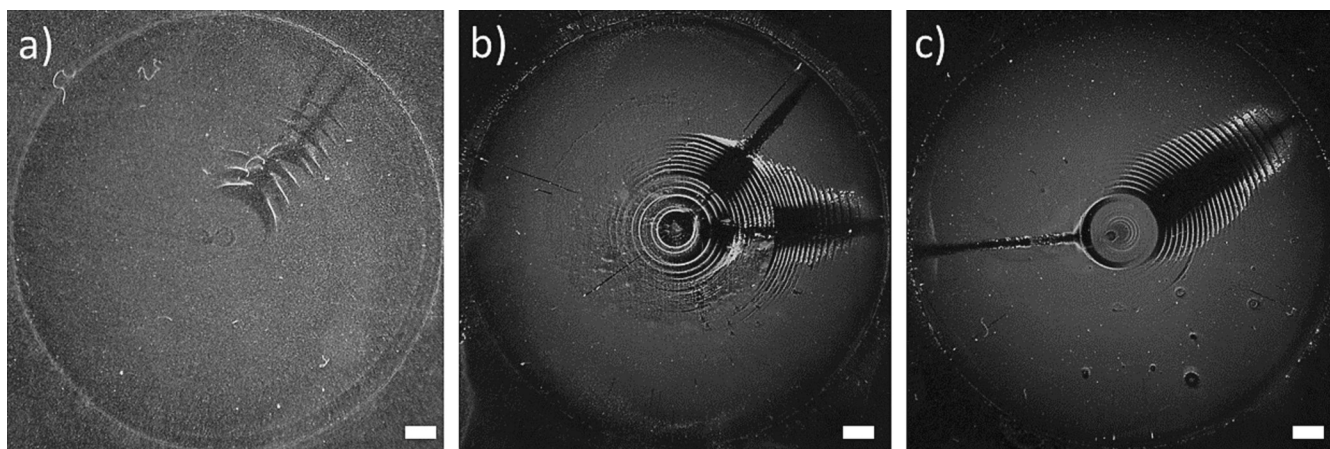
Fig. 4. Examples of changing the inlet channel during evaporation (observed with IPA). Panel (b) depicts an interesting event of a change of the inlet channel followed by a return to the initial one. The size of the scale bar (white line) is 1 mm.
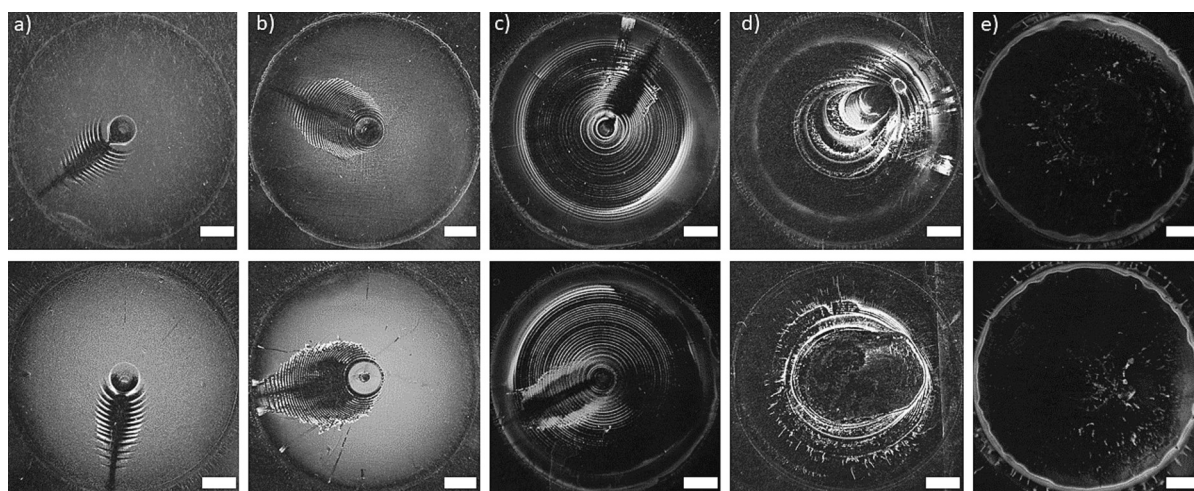

Fig. 5. Typical evaporation patterns obtained with various solvents: (a) isopropanol, (b) methanol, (c) ethanol (d), and (e) water. The suspensions were prepared with sub-micron DPs, except for (e) which was measured with 140 nm DPs. For each solution two representative patterns are presented. The size of the scale bar is 2 mm (white lines).
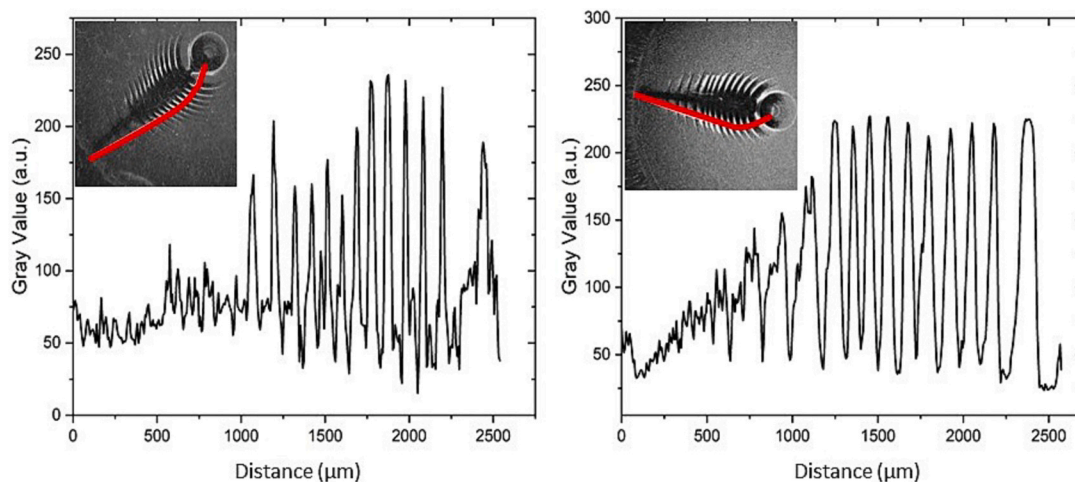

Fig. 6. Rib density profiles of DP-deposit patterns that occur with isopropanol and are presented in Fig. 5(a). The red lines in the insets depict the contours of a maximum modulation.

3.3.3. Impact of colloidal stability

On the basis of the investigated mechanism of the pattern development and structures obtained from the suspensions in different solvents, it may be stated that the colloidal properties of the diamond suspensions affect the deposition of diamond particles in the stripes form. The dispersion media affect the tendency of DPs to flocculate and sediment, which impacts their accumulation at the tip of the contact angle of the bottom liquid-air meniscus, and the formation of the ribs. Varied
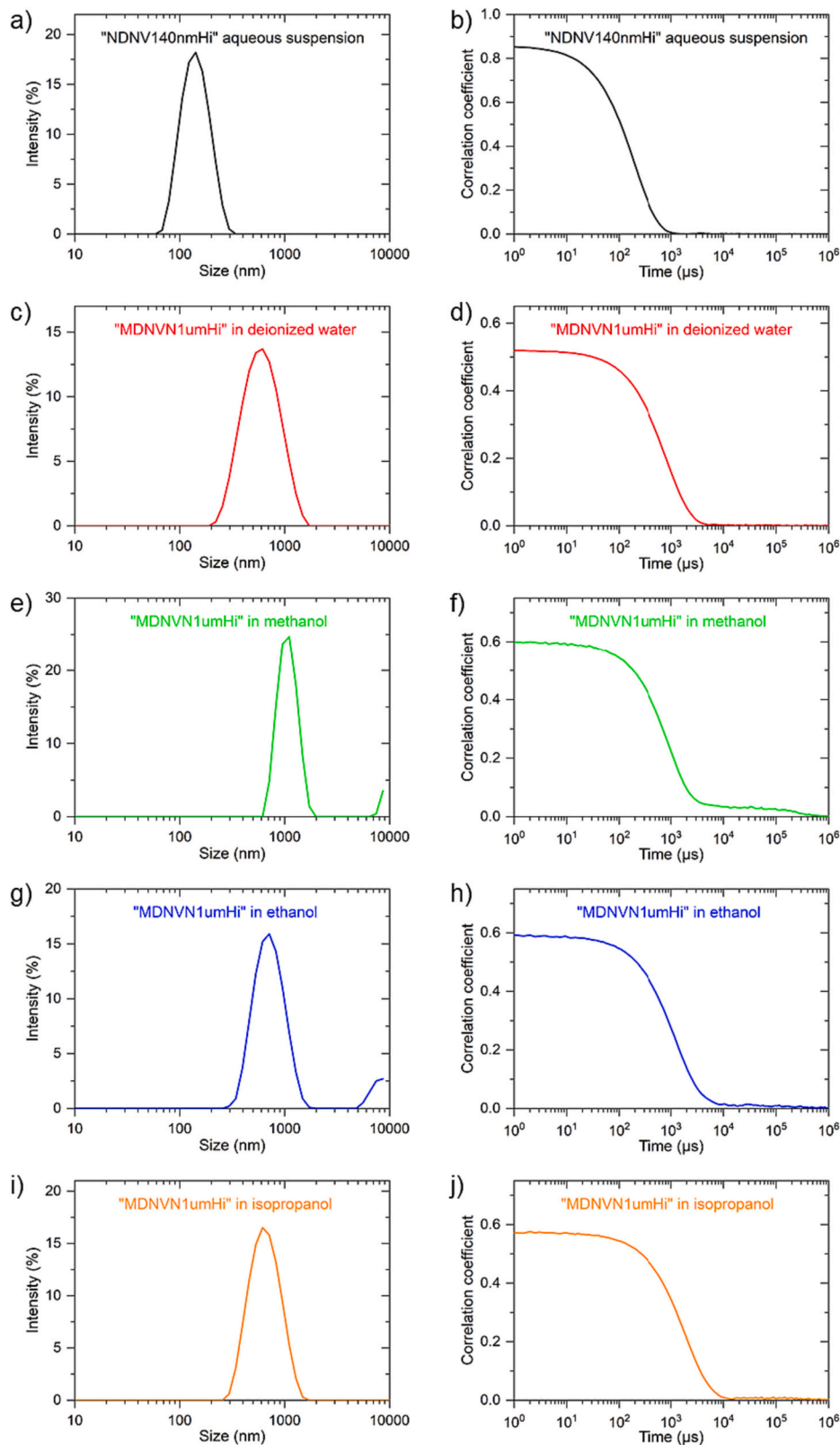

Fig. 7. Results of DLS measurements: particle size distributions (a, c, e, g, i) and correlograms (b, d, f, h, j) for aqueous suspension of "NDNV140nmHi" (a–b), and powdered "MDNVN1umHi" suspended in deionized water (c–d), methanol (e–f), ethanol (g–h), and isopropanol (i–j).

colloidal behavior of diamond particles dispersed in different media is visible in the results of dynamic light scattering (DLS) shown in Fig. 7.

The zeta potentials of the diamond particles along with the dynamic viscosities of their respective dispersion media are presented in Table 1. The vapor pressures of the solvents are also included in the table, as they serve as good indicators of the evaporation rate – a liquid characterized by a higher value of the vapor pressure evaporates more easily due to weak intermolecular forces [48]. Due to the presence of carboxyl moieties on their surfaces, non-modified diamond particles exhibit a negative zeta potential after being dispersed in liquids [49]. Diamonds suspended in deionized water are characterized by the zeta potentials of the highest magnitude. The values obtained for both the 140 nm-sized particles (−44.0 mV) and 700 nm-sized particles (−41.0 mV) indicate a high colloidal stability, confirmed in DLS measurements, which have yielded very repeatable results. The baselines of the correlograms in Fig. 7(b,d) are flat, which confirms that there should be no larger particles and/or agglomerates. Moreover, among the samples prepared from the "MDNVN1umHi" diamonds, the aqueous suspension is characterized by the smallest mean peak size of particles (Fig. 7(c)). Highly stable particles are not expected to sediment and accumulate at the bottom of the cavities. As water is assigned with the lowest vapor pressure among the investigated liquids, it is expected to evaporate relatively slowly. Expansion of the central air bubble in aqueous suspensions may be too slow to create a flow rate high enough to induce directional movement of the diamond particles. Therefore, ribs have not been formed in these cases and the chaotic structures probably result solely from the slow evaporation of water.

Of all the solvents used in the study, methanol is characterized by the lowest dynamic viscosity and the highest volatility due to the largest value of its vapor pressure. Both these properties facilitate fluctuations of the central air bubble and make DPs suspension prone to the recoil effect, resulting in irregularity of the deposited patterns. The DPs suspended in methanol are also characterized by the lowest absolute value of the zeta potential (−27.4 mV), and therefore the lowest colloidal stability among the investigated samples. The instability is further confirmed by the results of DLS measurements (Fig. 7(e,f)). The baseline in the correlogram in Fig. 7(f) is far from flat, with the correlation coefficient not reaching zero until very late, which indicates flocculation of DPs. The particle size distribution (Fig. 7(e)) reveals the presence of a larger fraction of the particles, which due to their size must undergo sedimentation. This fraction starts at ≈6.5 μm and extends beyond the detection limit (10 μm). The DPs suspended in methanol are expected to aggregate and flocculate rapidly throughout the liquid in its entire volume, additionally disturbing the orderliness/regularity of the fish skeleton-like patterns.

Because of its high dynamic viscosity, isopropanol is less prone to fluctuations and the recoil effect. Assessed by the value of the zeta potential (−29.0 mV), the stability of DPs dispersed in isopropanol is slightly higher compared to methanol, though the particles still show a tendency to sediment as displayed by the baseline of the correlogram

Table 1
Zeta potentials of diamond particles suspended in methanol, ethanol, isopropanol, and deionized water along with selected physical properties of the solvents.

	Zeta potential (mV)	Dynamic viscosity (cP) of solvent in 25 °C [50]	Vapor pressure (kPa) of solvent at 25 °C [50]
"MDNVN1umHi" powder suspended in			
Methanol	−27.4	0.544	16.9
Ethanol	−35.9	1.074	7.87
Isopropanol	−29.0	2.038	6.02
Deionized water	−41.0	0.89	3.169
"NDNV140nmHi" aqueous suspension	−44.0	0.89	3.169

(Fig. 7(j)) being noisy in comparison to the aqueous suspension. The diamond particles may accumulate at the tip of the contact angle of the bottom liquid-air meniscus, but their flocculation may occur less rapidly, enabling one to create regular patterns. At the same time, isopropanol does not evaporate as easily as methanol and ethanol (with a smaller value of the vapor pressure), which makes this colloidal system more stable and provides enough time for patterns to form.

3.3.4. Control experiments

We performed three control experiments and each of these measurements included three samples. In the first one, pure isopropanol was evaporated from a cavity slide sealed by a coverslip glass. This did not result in a formation of any fish-skeleton like deposit on the bottom of the well. A very thin and faint organic deposit from solvent was observed only along the edge of the cavity, and it did not show any fluorescence under excitation with 532-nm-wavelength light. The second control experiment included the evaporation of a diamond suspension in isopropanol from an uncovered well. Unconstrained evaporation from the whole cavity surface left a deposit with evenly distributed DPs. In the third control experiment, the slide well was filled halfway with DPs suspension in IPA and sealed with a glass coverslip. The obtained deposit also did not reproduce the regular and symmetric patterns of the fish skeleton-like structure.

4. Discussion

The main result of this work is the identification of mechanisms responsible for the development of structures deposited during confined evaporation of DPs suspensions with various solvents. These structures are the result of the interplay of several factors. Some are well known from other observations, like the Marangoni effect or coffee-ring, but some are novel caused by the specific conditions of the described experiment, like the confined evaporation in a specific well geometry, and/or directional air bubble flow. Although we managed to identify the basic mechanism, the phenomenon is very complex with the contribution of several synergistic mechanisms that were difficult to estimate quantitatively in the described experiments. For example, we observed oscillations of the liquid-air interface that could contribute to the overall dynamics. In our studies, we were focusing on diamond particles because of unique surface chemistry affecting assembly behavior, but we hope that the described mechanism of the pattern formation is a general one and can also occur in other cases.

In contrast to earlier observations, where the radially isotropic Marangoni flows were the main driving force, the effects analyzed here are mainly caused by gradual, confined evaporation and the directional flow of small air bubbles. Stimulated bubble and DPs flows appear to be the most relevant mechanisms that determine the properties of the deposited patterns. Although the flow starts stochastically from a random local leak in the liquid film between two glass surfaces, it determines a regular directional flow to the cavity center and the orientation of the final structure of the deposited pattern.

This study reveals that the orderliness and the regularity of the deposited patterns depend on a combination of several factors, among which there are zeta potential of the particles as well as dynamic viscosity and evaporation rate of the dispersion media. Terminal sedimentation velocity of particles suspended in liquids is directly proportional to their size and inversely proportional to the viscosity of the solvent [29]. Therefore, larger and/or aggregated diamonds are expected to flocculate more rapidly than well-dispersed particles. The size of the particles suspended in liquids is influenced by the zeta potential. Generally speaking, the higher the magnitude of the zeta potential, the stronger the electrostatic repulsion between the particles, and the more well-dispersed they stay. It should also be pointed out that the mathematics used by particle analyzers like the Zetasizer Nano ZS to determine zeta potential of the particles takes into consideration dynamic viscosity of the liquids. According to the equation used, the zeta

potential is directly proportional to the dynamic viscosity of the colloidal system [51]. The evaporation rate of the liquid impacts the inflow of air bubbles along the inlet channel and the expansion of the central air bubble, which results in the directional flow positioning the sedimenting particles at the bottom of the cavity.

The self-assembled patterns described in this study exhibit high spatial density modulation with the contrast reaching 100 % and reveal their potential for application. In particular, they could serve as substrates for selective-area nucleation and growth of diamond crystals using chemical vapor deposition. Moreover, if the observed mechanism of formation could be reproduced with electrically conductive diamond particles (e.g. boron-doped diamonds), the stripes might potentially be used as interdigitated electrodes.

5. Summary & conclusions

In summary, we have demonstrated the formation of concentric stripe patterns through a confined evaporation of an DPs suspension from a spherical cavity slide. A small bubble influx and strong, directional liquid circulation produced a residue with a periodic stripe pattern of diamond particles resembling a fish skeleton. These patterns were formed during the continuous and oscillatory motion of the liquid-air contact line due to the pinning-depinning (or stick and slip) mechanism.

The exact shape of the formed deposit strongly depends on the kind of solvent used. We observed the thinnest spine gap and the highest structure reproducibility with isopropanol, while the most characteristic feature of the ethanol patterns (Fig. 5(c)) were the ribs in the form of regular concentric rings broken by a well-visible regular spine without DPs. The patterns obtained with methanol also exhibited a distinct fish skeleton-like structure with a visible spine and ribs, but the ribs were wider and less regular than those of IPA and had irregular broken ends and visible gaps. These differences are attributed to the better colloidal stability of DPs dispersed in isopropyl alcohol. Unlike alcohols, water suspensions of sub-micron particles and 140 nm DPs did not result in regular and symmetric fish skeleton-like patterns. We have attributed this to a fairly good stability of diamond particles in water since these are not expected to sediment and accumulate at the bottom of the cavity.

The self-assembling processes of creating specific patterns of other particle types are still an open question. In our experiments, the critical parameters turned out to be the particle size and the kind of solvent. Although in our studies the choice of DPs was important because of two reasons: our future applications and the diamond particles' unique surface chemistry impacting its' assembly behavior, we believe that the described mechanism of the self-assembling process under conditions of constrained evaporation is to a large extent universal. Thus, we expect that sub-micrometer particles with a density close to that of diamond (3.5 g/cm^3), matched with a proper solvent, ensuring colloidal stability, could produce patterns similar to the ones discussed here. Specifically, interesting candidates could be particles of magnetite (Fe_3O_4, d = 5.1 g/cm^3), alumina (Al_2O_3, 4.0 g/cm^3), rutile (TiO_2, d = 4.26 g/cm^3), or zirconia (ZrO_2, d = 5.68 g/cm^3). Understanding the mechanism of formation of such a structure may also contribute to understanding of the processes of surface modification through the solvent.

Supplementary data to this article can be found online at https://doi.org/10.1016/j.diamond.2023.110783.

CRediT authorship contribution statement

Paulina Czarnecka-Trela: Conceptualization, Formal analysis, Investigation, Validation, Writing – original draft, Writing – review & editing. **Adam M. Wojciechowski:** Formal analysis, Supervision, Validation, Writing – review & editing. **Mariusz Mrózek:** Conceptualization, Formal analysis, Validation, Writing – review & editing. **Maciej J. Głowacki:** Formal analysis, Investigation, Methodology, Resources, Validation, Writing – review & editing. **Robert Bogdanowicz:** Formal

analysis, Resources, Supervision, Validation, Writing – review & editing. **Wojciech Gawlik:** Formal analysis, Funding acquisition, Methodology, Resources, Validation, Writing – original draft, Writing – review & editing.

Declaration of competing interest

We declare that we do not have any commercial or associative interest that represents a conflict of interest in connection with the work submitted.

Data availability

The data generated or analyzed during the current study are available from the corresponding author on reasonable request.

Acknowledgement

References

[1] Y.J. Chen, K. Suzuki, H. Mahara, T. Yamaguchi, Quasi-logarithmic spacing law in dewetting patterns from the drying meniscus of a polymer solution, Chem. Phys. Lett. 529 (2012) 74–78, https://doi.org/10.1016/j.cplett.2012.01.046.

[2] N.J. Suematsu, Y. Ogawa, Y. Yamamoto, T. Yamaguchi, Dewetting self-assembly of nanoparticles into hexagonal array of nanorings, J. Colloid Interface Sci. 310 (2) (2007) 648–652, https://doi.org/10.1016/J.JCIS.2007.02.037.

[3] R.A. Farrell, N. Kehagias, M.T. Shaw, V. Reboud, M. Zelsmann, J.D. Holmes, C.M.S. Torres, M.A. Morris, Surface-directed dewetting of a block copolymer for fabricating highly uniform nanostructured microdroplets and concentric nanorings, ACS Nano 5 (2) (2011) 1073–1085, https://doi.org/10.1021/nn102720m.

[4] Kuniaki Nagayama Eiki Adachi ASD, Stripe patterns formed on a glass surface during droplet evaporation, Langmuir 11 (1995) 1057–1060.

[5] O. Karthaus, L. Gråsjö, N. Maruyama, M. Shimomura, Formation of ordered mesoscopic polymer arrays by dewetting, Chaos 9 (2) (1999) 308–314, https://doi.org/10.1063/1.166407.

[6] B.M. Weon, J.H. Je, Capillary force repels coffee-ring effect, Phys. Rev. E Stat. Nonlinear Soft Matter Phys. 82 (1) (2010) 1–4, https://doi.org/10.1103/PhysRevE.82.015305.

[7] Y.J. Chen, K. Suzuki, H. Mahara, K. Yoshikawa, T. Yamaguchi, Self-organized Archimedean spiral pattern: regular bundling of fullerene through solvent evaporation, Appl. Phys. Lett. 102 (4) (2013) 1–15, https://doi.org/10.1063/1.4789906.

[8] J. Lian, L. Wang, X. Sun, Q. Yu, R.C. Ewing, Patterning metallic nanostructures by ion-beam-induced dewetting and Rayleigh instability, Nano Lett. 6 (11) (2006) 2637, https://doi.org/10.1021/nl068002q.

[9] Y. Lin, Z. Su, E. Balizan, Z. Niu, Q. Wang, Controlled assembly of protein in glass capillary, Langmuir 26 (15) (2010) 12803–12809, https://doi.org/10.1021/la1017888.

[10] K. Kolegov, L. Barash, Applying droplets and films in evaporative lithography, Adv. Colloid Interf. Sci. 285 (2020) 102271, https://doi.org/10.1016/j.cis.2020.102271.

[11] H. Wei, X. Zhao, Y. Wei, H. Ma, D. Li, G. Chen, H. Lin, S. Fan, K. Jiang, Flash-evaporation printing methodology for perovskite thin films, NPG Asia Mater. 9 (6) (2017) e395, https://doi.org/10.1038/am.2017.91.

[12] S. Lone, J. Zhang, I.U. Vakarelski, E. Li, S.T. Thoroddsen, Evaporative lithography in open microfluidic channel networks, Langmuir (2017), https://doi.org/10.1021/acs.langmuir.6b03304.

[13] P. Kralchevsky, K. Nagayama, Capillary bridges and capillary-bridge forces, in: Studies in Interface Science 10, 2001, pp. 469–502, https://doi.org/10.1016/S1383-7303(01)80052-1.

[14] J. Xu, J. Xia, S.W. Hong, Z. Lin, F. Qiu, Y. Yang, Self-assembly of gradient concentric rings via solvent evaporation from a capillary bridge, Phys. Rev. Lett. 96 (6) (2006) 66104, https://doi.org/10.1103/PhysRevLett.96.066104.

[15] S. Ogoshi, M. Ueta, T. Arai, H. Kurosawa, AlMe3-promoted oxidative cyclization of η2-alkene and η2-ketone on nickel(0). Observation of intermediate in methyl transfer process, J. Am. Chem. Soc. 127 (37) (2005) 12810–12811, https://doi.org/10.1021/ja0542486.

[16] W.K. Park, T. Kim, H. Kim, Y. Kim, T.T. Tung, Z. Lin, A.R. Jang, H.S. Shin, J.H. Han, D.H. Yoon, W.S. Yang, Large-scale patterning by the roll-based evaporation-induced self-assembly, J. Mater. Chem. 22 (43) (2012) 22844–22847, https://doi.org/10.1039/C2JM34212J.

[17] H. Hu, R.G. Larson, Evaporation of a sessile droplet on a substrate, J. Phys. Chem. B 106 (6) (2002) 1334–1344, https://doi.org/10.1021/jp0118322.

[18] H. Hu, R.G. Larson, Marangoni effect reverses coffee-ring depositions, J. Phys. Chem. B 110 (14) (2006) 7090–7094, https://doi.org/10.1021/jp0609232.

[19] W.D. Ristenpart, P.G. Kim, C. Domingues, J. Wan, H.A. Stone, Influence of substrate conductivity on circulation reversal in evaporating drops, Phys. Rev. Lett. 99 (23) (2007) 234502, https://doi.org/10.1103/PhysRevLett.99.234502.

[20] B. Rajneesh, F. Xiaohua, A. Daniel, Pattern Formation during the Evaporation of a Colloidal Nanoliter Drop: A Numerical and Experimental Study. 11 (2009). http s://arxiv.org/pdf/1010.2560.pdf%0Ahttp://stacks.iop.org/1367-2630/11/i=7/a =075020.

[21] M. Wu, X. Man, M. Doi, Multi-ring deposition pattern of drying droplets, Langmuir 34(32):9572-9578 (2018), https://doi.org/10.1021/acs.langmuir.8b01655.

[22] D. Mampallil, H.B. Eral, A review on suppression and utilization of the coffee-ring effect, Adv. Colloid Interf. Sci. 252 (2018) 38–54, https://doi.org/10.1016/j. cis.2017.12.008.

[23] H. Kim, F. Boulogne, E. Um, I. Jacobi, E. Button, H.A. Stone, Controlled uniform coating from the interplay of Marangoni flows and surface-adsorbed macromolecules, Phys. Rev. Lett. 116 (12) (2016) 124501, https://doi.org/ 10.1103/PhysRevLett.116.124501.

[24] H. Huang, L. Dai, D.H. Wang, L.S. Tan, E. Osawa, Large-scale self-assembly of dispersed nanodiamonds, J. Mater. Chem. 18 (12) (2008) 1347–1352, https://doi. org/10.1039/B716676A.

[25] C. Seo, D. Jang, J. Chae, S. Shin, Altering the coffee-ring effect by adding a surfactant-like viscous polymer solution, Sci. Rep. 7 (1) (2017) 500, https://doi. org/10.1038/s41598-017-00497-x.

[26] M.J. Głowacki, M. Ficek, M. Sawczak, A. Wcisło, R. Bogdanowicz, Fluorescence of nanodiamond cocktails: pH-induced effects through interactions with comestible liquids, Food Chem. 381 (2022) 132206, https://doi.org/10.1016/j. foodchem.2022.132206.

[27] V. Jirásek, Š. Stehlík, P. Štenclová, A. Artemenko, B. Rezek, A. Kromka, Hydroxylation and self-assembly of colloidal hydrogenated nanodiamonds by aqueous oxygen radicals from atmospheric pressure plasma jet, RSC Adv. 8 (66) (2018) 37681–37692, https://doi.org/10.1039/c8ra07873d.

[28] S.L.Y. Chang, P. Reineck, D. Williams, G. Bryant, G. Opletal, S.A. El-Demrdash, P. L. Chiu, E. Osawa, A.S. Barnard, C. Dwyer, Dynamic self-assembly of detonation nanodiamond in water, Nanoscale 12 (9) (2020) 5363–5367, https://doi.org/ 10.1039/c9nr08984e.

[29] T. Yoshikawa, M. Liu, S.L.Y. Chang, I.C. Kuschnerus, Y. Makino, A. Tsurui, T. Mahiko, M. Nishikawa, Steric interaction of polyglycerol-functionalized detonation nanodiamonds, Langmuir 38 (2) (2022) 661–669, https://doi.org/ 10.1021/acs.langmuir.1c02283.

[30] S.A. El-Demrdash, R. Nixon-Luke, L. Thomsen, A. Tadich, D.W.M. Lau, S.L. Y. Chang, T.L. Greaves, G. Bryant, P. Reineck, The effect of salt and particle concentration on the dynamic self-assembly of detonation nanodiamonds in water, Nanoscale 13 (33) (2021) 14110–14118, https://doi.org/10.1039/d1nr04847c.

[31] G. Opletal, S.L. Chang, A.S. Barnard, Simulating facet-dependent aggregation and assembly of distributions of polyhedral nanoparticles, Nanoscale 12 (38) (2020) 19870–19879, https://doi.org/10.1039/d0nr03470c.

[32] H.J. Shulevitz, T.Y. Huang, J. Xu, S.J. Neuhaus, R.N. Patel, Y.C. Choi, L.C. Bassett, C.R. Kagan, Template-assisted self-assembly of fluorescent nanodiamonds for scalable quantum technologies, ACS Nano 16 (2) (2022) 1847–1856, https://doi. org/10.1021/acsnano.1c09839.

[33] Y. Li, J. Lu, X. Deng, X. Wang, F. Jia, S. Zhong, X. Cui, Z. Pan, L. Shao, Y. Wu, Self-assembling combretastatin A4 incorporated protamine/nanodiamond hybrids for combined anti-angiogenesis and mild photothermal therapy in liver cancer, Nanotechnology 32 (46) (2021) 465101, https://doi.org/10.1088/1361-6528/ ac1be0.

[34] L. Liang, P. Zheng, S. Jia, K. Ray, Y. Chen, I. Barman, DNA Self-Assembled Plasmonic Nanodiamonds for Biological Sensing. bioRxiv, November 11, 2021, https://doi.org/10.1101/2021.11.09.467982 (2021.11.09.467982).

[35] L. Schmidheini, R.F. Tiefenauer, V. Gatterdam, A. Frutiger, T. Sannomiya, M. Aramesh, Self-assembly of nanodiamonds and plasmonic nanoparticles for nanoscopy, Biosensors 12 (3) (2022) 148, https://doi.org/10.3390/bios12030148.

[36] N.M. Kuznetsov, A.Y. Vdovichenko, A.V. Bakirov, S.I. Belousov, R.A. Kamyshinsky, A.L. Vasiliev, E.S. Kulikova, R.D. Svetogorov, S.N. Chvalun, E.B. Yudina, A.Y. Vul', The size effect of faceted detonation nanodiamond particles on electrorheological behavior of suspensions in mineral oil, Diam. Relat. Mater. 125 (2022) 108967, https://doi.org/10.1016/J.DIAMOND.2022.108967.

[37] I.C. Kuschnerus, H. Wen, X. Zeng, Y.Y. Khine, J. Ruan, C.J. Su, U.S. Jeng, H. A. Girard, J.C. Arnault, E. Ōsawa, O. Shenderova, V.N. Mochalin, M. Liu, M. Nishikawa, S.L.Y. Chang, Fabrication process independent and robust aggregation of detonation nanodiamonds in aqueous media, Diam. Relat. Mater. 139 (2023) 110199, https://doi.org/10.1016/J.DIAMOND.2023.110199.

[38] K. Kolarova, I. Bydzovska, O. Romanyuk, E. Shagieva, E. Ukraintsev, A. Kromka, B. Rezek, S. Stehlik, Hydrogenation of HPHT nanodiamonds and their nanoscale interaction with chitosan, Diam. Relat. Mater. 134 (2023) 109754, https://doi.org/ 10.1016/J.DIAMOND.2023.109754.

[39] N.H. Patoary, A. Rai, K.P. Patel, A. Rebecca, W. Zhang, A.J. Ulrich, M. Galib, T. Desai, S. Zivanovic, M. Yousufuddin, A.L. Moore, A.D. Radadia, Directed covalent assembly of nanodiamonds into thin films, Diam. Relat. Mater. 101 (2020) 107605, https://doi.org/10.1016/J.DIAMOND.2019.107605.

[40] Zetasizer Nano user manual (English) | Malvern Panalytical. https://www.malve rnpanalytical.com/en/learn/knowledge-center/user-manuals/man0485en. (Accessed 23 October 2022).

[41] R.D. Deegan, O. Bakajin, T.F. Dupont, G. Huber, S.R. Nagel, T.A. Witten, Capillary flow as the cause of ring stains from dried liquid drops, Nature 389 (6653) (1997) 827–829, https://doi.org/10.1038/39827.

[42] C. Cohen, F. Restagno, C. Poulard, L. Léger, Wetting and dewetting transition: an efficient toolbox for characterizing low-energy surfaces, Langmuir 26 (19) (2010) 15345–15349, https://doi.org/10.1021/LA102545Z/ASSET/IMAGES/MEDIUM/ LA-2010-02545Z_0005.GIF.

[43] F. Restagno, C. Poulard, C. Cohen, L. Vagharchakian, L. Léger, Contact angle and contact angle hysteresis measurements using the capillary bridge technique, Langmuir 25 (18) (2009) 11188–11196, https://doi.org/10.1021/LA901616X/ ASSET/IMAGES/MEDIUM/LA-2009-01616X_0014.GIF.

[44] P.G. de Gennes, F. Brochard-Wyart, D. Quéré, Capillarity and wetting phenomena, in: Capillarity and Wetting Phenomena, 2004, https://doi.org/10.1007/978-0- 387-21656-0.

[45] S. Wu, Y. He, Q. Zheng, M. Ma, Oscillating friction of nanoscale capillary bridge, Friction 10 (2) (2022) 200–208, https://doi.org/10.1007/S40544-020-0396-X/ METRICS.

[46] Y.J. Chen, K. Suzuki, K. Yoshikawa, Self-organized target and spiral patterns through the "coffee ring" effect, J. Chem. Phys. 143 (8) (2015), https://doi.org/ 10.1063/1.4929341.

[47] B.M. Weon, J.H. Je, Fingering inside the coffee ring, Phys. Rev. E 87 (1) (2013) 13003, https://doi.org/10.1103/PhysRevE.87.013003.

[48] D. Mackay, I. Van Wesenbeeck, Correlation of chemical evaporation rate with vapor pressure, Environ. Sci. Technol. 48 (17) (2014) 10259–10263, https://doi. org/10.1021/ES5029074/ASSET/IMAGES/MEDIUM/ES-2014-029074_0005.GIF.

[49] M. Janik, M.J. Głowacki, M. Sawczak, A. Wcisło, P. Niedziałkowski, K. Jurak, M. Ficek, R. Bogdanowicz, Poly-l-lysine-functionalized fluorescent diamond particles: pH triggered fluorescence enhancement via surface charge modulation, MRS Bull. 47 (10) (2022) 1011–1022, https://doi.org/10.1557/S43577-022- 00326-1/METRICS.

[50] CRC Handbook of Chemistry and Physics, 87th ed Editor-in-Chief: David R. Lide (National Institute of Standards and Technology), CRC Press/Taylor and Francis Group, Boca Raton, FL, 2006, https://doi.org/10.1021/ja069813z (2608 pp. 139.95. ISBN 0-8493-0487-3. J Am Chem Soc. 2007;129(3):724).

[51] G.V. Lowry, R.J. Hill, S. Harper, A.F. Rawle, C.O. Hendren, F. Klaessig, U. Nobbmann, P. Sayre, J. Rumble, Guidance to improve the scientific value of zeta-potential measurements in nanoEHS, Environ. Sci. Nano 3 (5) (2016) 953–965, https://doi.org/10.1039/C6EN00136J.